PNAS
www.pnas.org

Supplementary Information for

Molecular basis of Coxsackievirus A10 entry using the two-in-one attachment and uncoating receptor KRM1

Yingzi Cui, Ruchao Peng, Hao Song, Zhou Tong, Xiao Qu, Sheng Liu, Xin Zhao, Yan Chai, Peiyi Wang, George F. Gao, and Jianxun Qi

Corresponding authors: George F. Gao & Jianxun Qi
Email: gaof@im.ac.cn (G.F.G.); jxqi@im.ac.cn (J.Q.)

This PDF file includes:

> Supplementary text
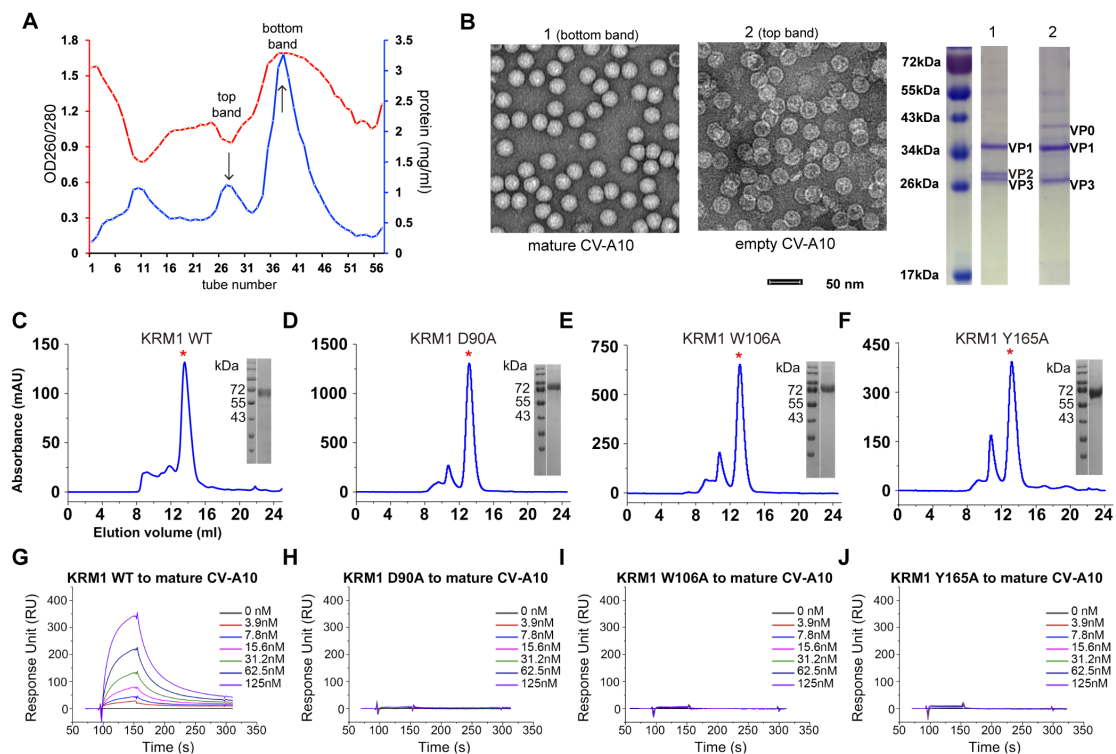> Figures S1 to S10
> Tables S1 to S2

1

Fig. S1. Purification and biochemical characterization of CV-A10 virus and KRM1 proteins. (*A*) Virus quality test after sucrose gradient cushion purification. The two peaks (indicated by black arrows) were collected and subjected to further analysis. The first peak (top band) mainly consisted of empty capsid particles, and the second peak (bottom band) was mainly composed of mature virions with a high OD260/280 absorbance ratio due to the presence of the RNA genome. **(*B*)** Negative-stain EM micrographs and SDS-PAGE profiles of the mature (lane 1) and empty (lane 2) CV-A10 viral particles. **(*C-F*)** SEC profiles of KRM1 proteins using a Superdex 200 10/300 GL column. Predicted monomeric molecules are eluted around 13.5 mL, labeled by a red asterisk, and peaks were then analyzed by SDS-PAGE. **(*G-J*)** The binding curves of KRM1 and its mutants to immobilized CV-A10 at physiological pH, corresponding to **(*C-F*)**, respectively. The data were analyzed with BIAcore 3000 Evaluation software (GE Healthcare). The results shown are representatives of three independent experiments.
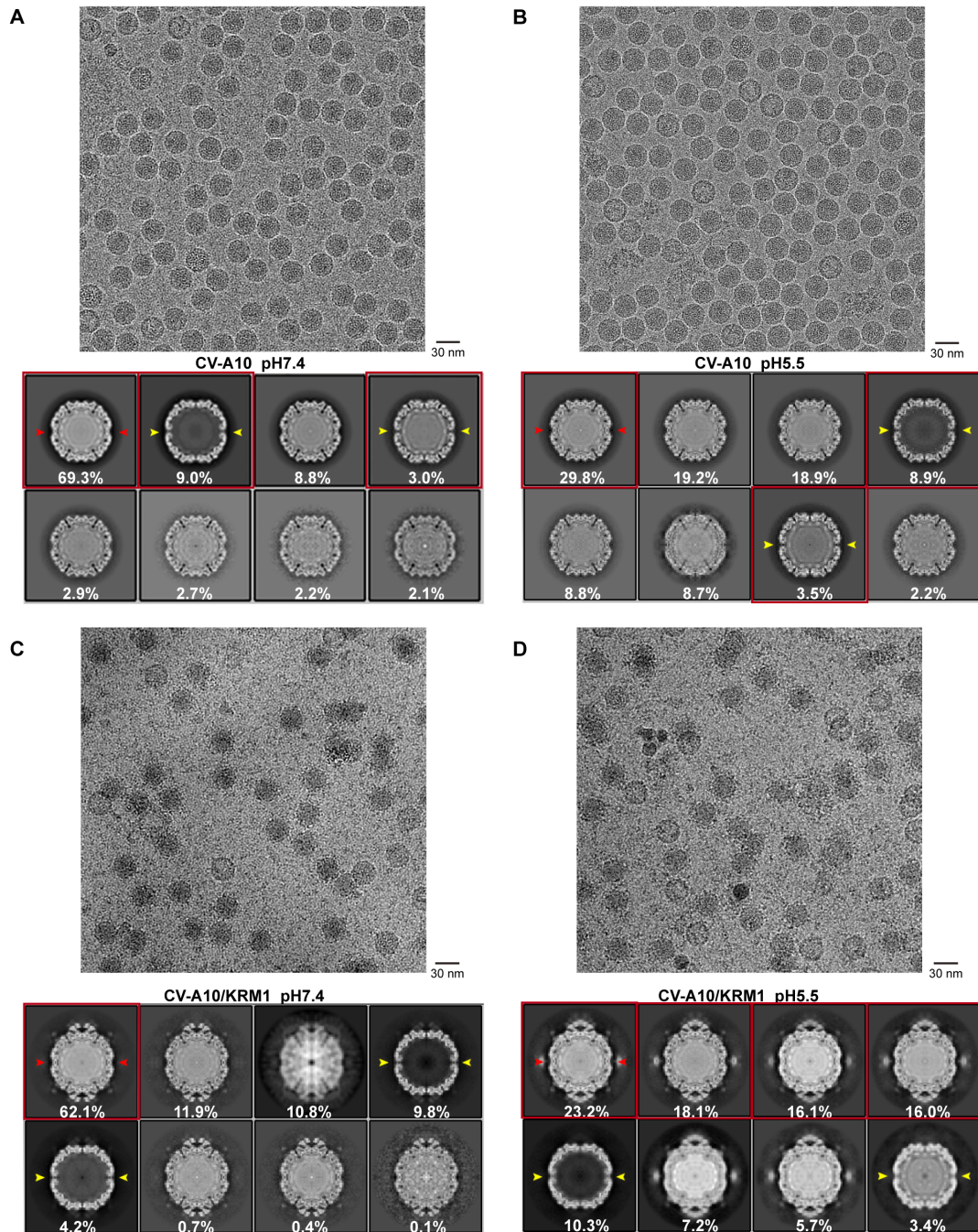
Fig. S2. Cryo-EM images and 3D classification results of CV-A10 virus and its complex with KRM1. (*A* and *B*) Representative micrographs (upper panel) and 3D class average images (lower panel) of CV-A10 particles at pH 7.4 (*A*) or pH 5.5 (*B*). A-particles and empty particles could be obviously distinguished from mature virus through the open

channels in the two-fold axis (indicates by yellow arrows), which were closed in the mature virus (red arrows). The virus preparation was mainly composed of mature virions (>80%). **(*C* and *D*)** Representative micrographs and 3D class average images of CV-A10 in the presence of KRM1 at pH 7.4 (***C***) or pH 5.5 (***D***).
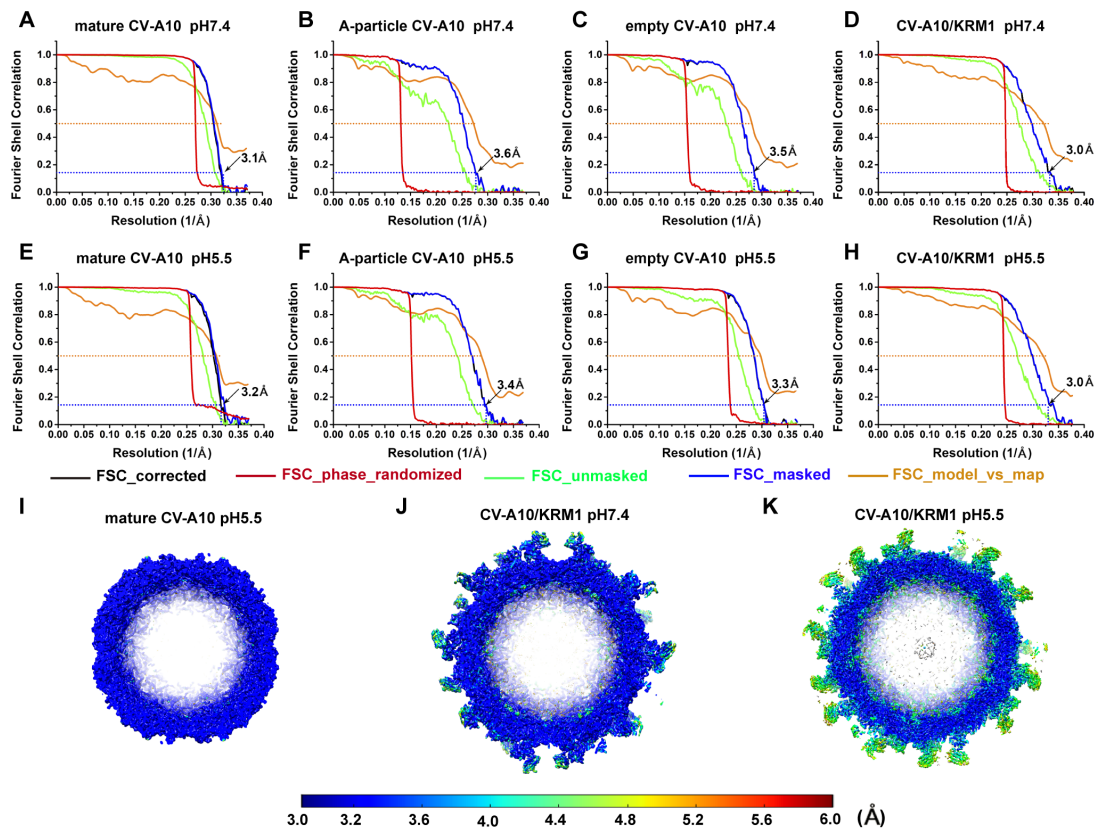
Fig. S3. Resolution evaluations for EM maps of CV-A10 virus and its complex with KRM1. (*A-H*) Fourier shell correlation (FSC) of the final 3D reconstruction obtained using gold-standard refinement in Relion. The 0.143 and 0.5 FSC cut-off values are indicated by blue and orange dashed lines, respectively. (***I-K***) Local resolution maps of representative density maps of CV-A10 virus or its complex with KRM1. In all of these structures, most core regions reached 3.0 Å and allowed the atomic details to be resolved.
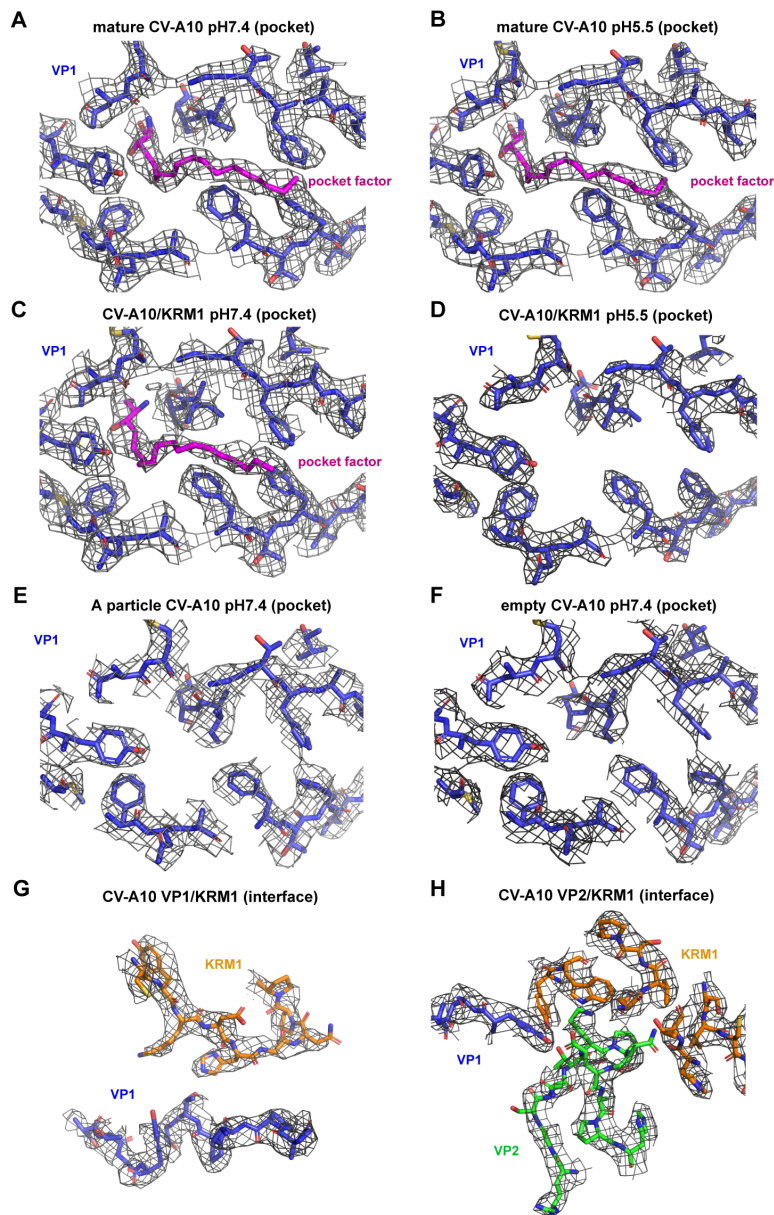
Fig. S4. Representative density maps of the pocket region and receptor-binding interface. (*A-B*) The "pocket factor" is preserved in structures of mature CV-A10 in both neutral and acidic conditions. (*C-D*) With receptor-binding, the occupancy of "pocket factor" is reduced at pH 7.4 and almost drops to zero at pH 5.5. (*E-F*) Collapsed pocket without "pocket factor" in A-particles and empty particle CV-A10 viruses. (*G-H*) In the receptor-binding interface, most side chains of key residues are resolved.
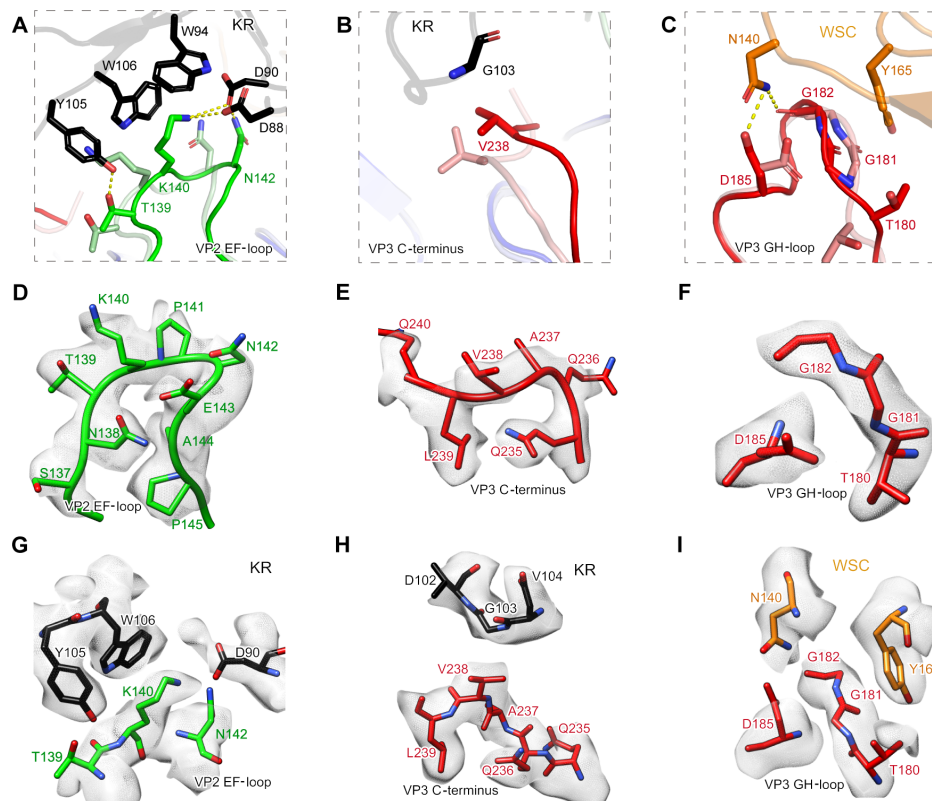
Fig. S5. Details of conformational shifts of capsid proteins upon receptor binding. (*A-C*) The interaction details depicting the reasons for conformational shifts caused by KRM1 binding. The proteins are colored by chains, and the critical interacting residues are displayed as sticks and colored by elements. Yellow dashed lines represent hydrogen bonds. (***D-F***) Cryo-EM density maps of mature CV-A10 viral capsid proteins at the receptor binding interface. (***G-I***) The density of corresponding contacting interface in the CV-A10/KRM1 complex at pH 7.4. Most of the amino acid side chains are clearly resolved in the density map. The interactions between contacting residues at the interface could be confidently defined.
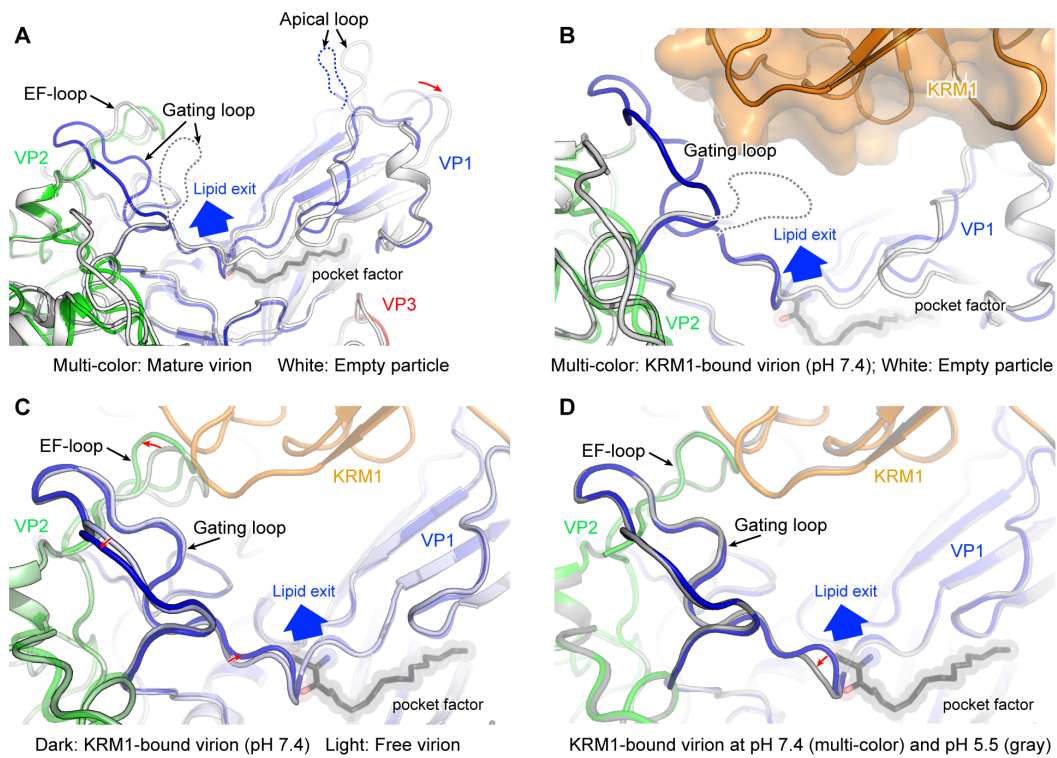
Fig. S6. Structural comparison of CV-A10 viral particles at different states/conditions.
(***A***) Comparison of CV-A10 mature virion (colored by proteins) with the empty capsid
(white) at pH 7.4. The VP2 EF-loop and the VP1 apical domain display different
conformations between the two structures. The VP1 gating loop is disordered (gray dashed
line) in the empty capsid in which the "pocket factor" is released. The lipid exit within the
canyon is indicated by a thick blue arrow. (***B***) Overlay of empty capsid (white) with the
KRM1-bound mature virion (colored by proteins) at pH 7.4. The KRM1-interacting gating
loop is disordered in the empty capsid. (***C***) Comparison of CV-A10 mature virion with
(dark colors) or without (light colors) KRM1 binding at pH 7.4. (***D***) Comparison of KRM1-
bound CV-A10 virion at pH 7.4 (in multiple colors) and pH 5.5 (gray) conditions.
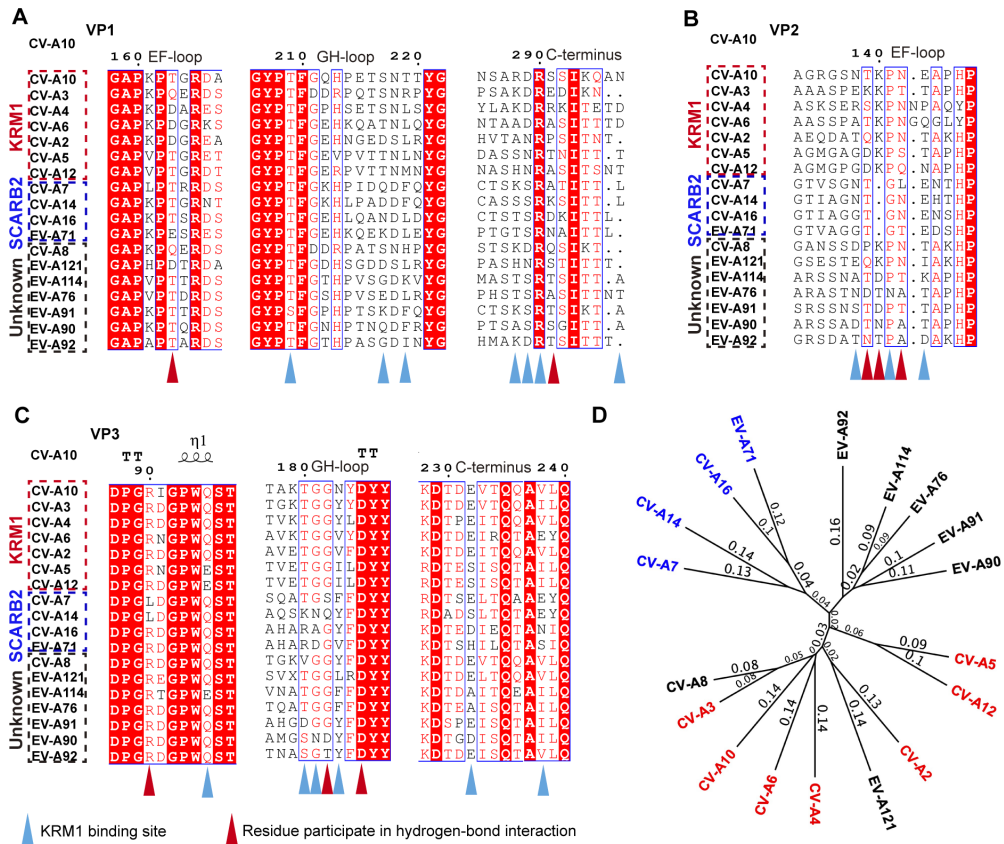
Fig. S7. Sequence alignments of infectious EV-As around the KRM1 binding site of CV-A10. (*A-C*) Symbolic epitomes of sequence alignment of CV-A10 VP1 (**A**), VP2 (**B**), and VP3 (**C**) in EV-As. The red triangles indicate amino acids that potentially participate in hydrogen-bond interactions with KRM1, while blue triangles indicate amino acids that contribute to other interaction patterns with KRM1. (**D**) Phylogenetic tree of the EV-As derived by comparing the P1 region (VP4, VP2, VP3, and VP1). Viruses using KRM1 and SCARB2 as receptors are highlighted in red and blue, respectively. GenBank Accession codes: CV-A10 (MT263729); CV-A3 (AY421761.1); CV-A4 (AY421762.1); CV-A6(AY421764.1); CV-A2 (AY421760.1); CV-A5 (AY421763.1); CV-A12 (AY421768.1); CV-A7 (AY421765.1); CV-A14 (AY421769.1); CV-A16 (KM055004.1); EV-A71(U22522.1); CV-A8 (AY421766.1); EV-A121 (NC_030454.1); EV-A114 (KU355877.1); EV-A76 (JF905564.1); EV-A91 (AY697461.1); EV-A90 (JX390655.1); and EV-A92 (EF667344.1). The sequence alignment and the phylogenetic tree were produced by ESPript and Geneious.

9
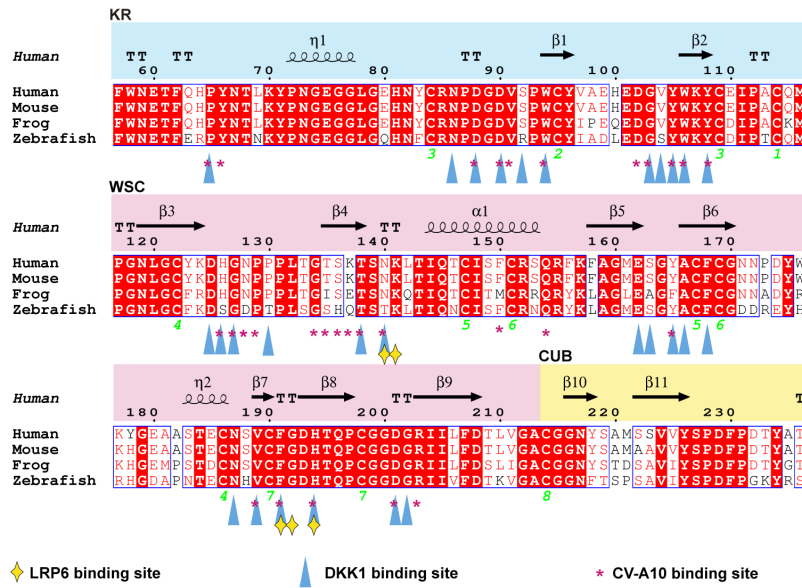
Fig. S8. Secondary structures and sequence alignment of KRM1 in different species. Residue numbering scheme based on that for human KRM1 and the secondary structure elements shown at the top of the alignment. The yellow diamond and blue triangle indicate LRP6 and DKK1 binding sites, respectively, and red asterisks highlight the CV-A10 binding site. Participating residues were analyzed by the contact program in CCP4 suite (the distance cutoff is 4.5 Å). GenBank Accession codes: KRM1 *Homo sapiens* (AAH63787); KRM1 *Mus musculus* (AAH82546); KRM1 *Xenopus laevis* (NP_001082145); and KRM1 *Danio rerio* (NP_001108389). The sequence alignment was produced by ESPript.
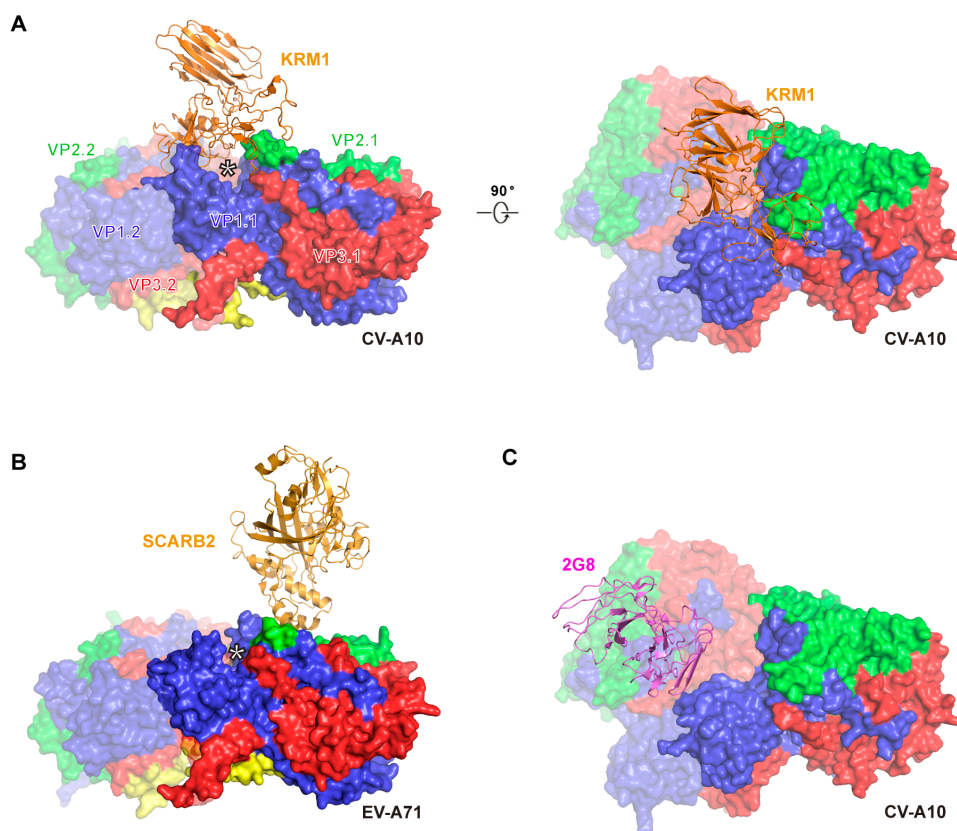
Fig. S9. Structural comparisons of the CV-A10/KRM1 binding mode to the EV-A71/SCARB2 or CV-A10/2G8 fab complex. (*A*) Side view (left) and top view (right) of the CV-A10/KRM1 complex, demonstrating the binding site of KRM1 to CV-A10. KRM1 binds to the top of the canyon, crossing two asymmetric units. (*B*) SCARB2 binds to the southern rim of the canyon. The canyon is highlighted with a white asterisk. (*C*) Epitope of 2G8 maps to all three capsid proteins (VP1 to VP3) in a single asymmetric unit. The viral proteins are shown in surface models (ASU.2 shown as a transparent surface), and the receptors/antibodies are shown as ribbons.
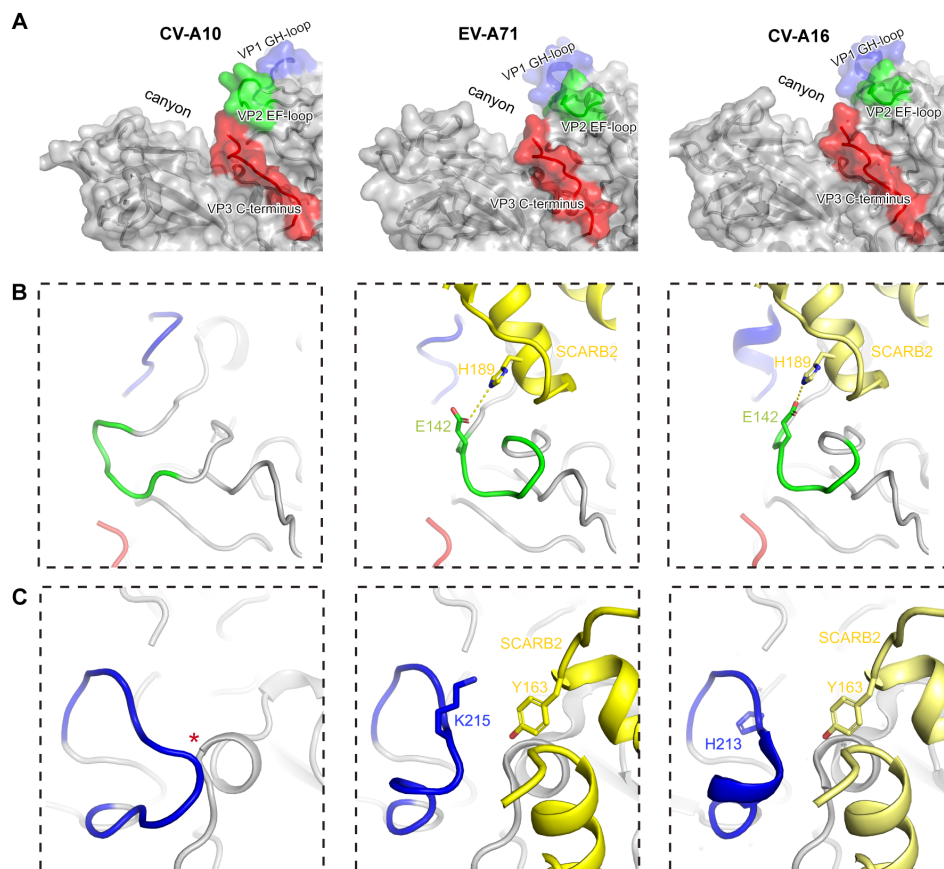
Fig. S10. Structure comparison of CV-A10, EV-A71, and CV-A16 receptor binding sites. (*A*) Surfaces of the viral capsid of CV-A10, EV-A71 (PDB: 6I2K), and CV-A16 (PDB: 5C4W) around the canyon walls. The VP1 GH-loop, VP2 EF-loop, and VP3 C-terminus are highlighted in blue, green, and red, respectively. (***B* and *C***) Close-up views of the VP2 EF-loop and VP1 GH-loop participating in the SCARB2 interaction. The SCARB2 is colored in yellow in the EV-A71/SCARB2 complex, and the aligned SCARB2 with CV-A16 is colored in pale yellow for distinction. The red asterisk highlights the possible steric hindrance imposed by the VP1 GH-loop in SCARB2-binding.

Table S1. Cryo-EM data collection, refinement, and validation statistics.

	CV-A10 mature particle (pH7.4)	CV-A10 mature particle (pH5.5)
Data collection and processing		
Magnification	37037	37037
Voltage (kV)	300	300
Electron exposure ($e^-/Å^2$)	40	40
Defocus range (μm)	-1.5 to -2.5	-1.5 to -2.5
Pixel size (Å)	1.35	1.35
Symmetry imposed	Icosahedral	Icosahedral
Initial particle images (no.)	59833	99876
Final particle images (no.)	38570	22864
Map resolution (Å)	3.1	3.2
FSC threshold	0.143	0.143
Map resolution range (Å)	3.0-6.0	3.0-6.0
Refinement		
Initial model used (PDB code)	6ACU	6ACU
Model resolution (Å)	3.2	3.2
Model resolution range (Å)	Up to 3.1	Up to 3.2
Map sharpening B factor ($Å^2$)	-141	-108
Model map FSC (masked)	0.85	0.82
Model composition		
Non-hydrogen atoms	6245	6180
Protein residues	800	793
Ligands	1	1
B factors ($Å^2$)		
Protein	28	30
Ligand	25	27
R.m.s. deviations		
Bond lengths (Å)	0.003	0.003
Bond angles (°)	0.65	0.62
Validation		
MolProbity score	2.32	2.24
Clashscore	7.39	9.75
Poor rotamers (%)	5.57	3.11
Ramachandran plot		
Favored (%)	94.94	94.88
Allowed (%)	4.94	4.99
Disallowed (%)	0.12	0.13

Table S1. Cryo-EM data collection, refinement, and validation statistics (continued).

	CV-A10 A-particle (pH7.4)	CV-A10 A-particle (pH5.5)
Data collection and processing		
Magnification	37037	37037
Voltage (kV)	300	300
Electron exposure ($e^-/\text{Å}^2$)	40	40
Defocus range (μm)	-1.5 to -2.5	-1.5 to -2.5
Pixel size (Å)	1.35	1.35
Symmetry imposed	Icosahedral	Icosahedral
Initial particle images (no.)	59833	99876
Final particle images (no.)	1786	2940
Map resolution (Å)	3.6	3.4
FSC threshold	0.143	0.143
Map resolution range (Å)	3.0-6.0	3.0-6.0
Refinement		
Initial model used (PDB code)	6ACU	6ACU
Model resolution (Å)	3.7	3.5
Model resolution range (Å)	Up to 3.6	Up to 3.4
Map sharpening B factor (Å^2)	-96	-98
Model map FSC (masked)	0.85	0.85
Model composition		
Non-hydrogen atoms	5109	5141
Protein residues	653	656
Ligands	0	0
B factors (Å^2)		
Protein	50	34
Ligand	-	-
R.m.s. deviations		
Bond lengths (Å)	0.003	0.004
Bond angles (°)	0.63	0.69
Validation		
MolProbity score	2.26	2.52
Clashscore	11.47	8.75
Poor rotamers (%)	2.14	7.28
Ramachandran plot		
Favored (%)	93.27	94.10
Allowed (%)	6.57	5.75
Disallowed (%)	0.16	0.15

Table S1. Cryo-EM data collection, refinement, and validation statistics (continued).

	CV-A10 empty particle (pH7.4)	CV-A10 empty particle (pH5.5)
Data collection and processing		
Magnification	37037	37037
Voltage (kV)	300	300
Electron exposure (e⁻/Å²)	40	40
Defocus range (μm)	-1.5 to -2.5	-1.5 to -2.5
Pixel size (Å)	1.35	1.35
Symmetry imposed	Icosahedral	Icosahedral
Initial particle images (no.)	59833	99876
Final particle images (no.)	5179	8877
Map resolution (Å)	3.5	3.3
FSC threshold	0.143	0.143
Map resolution range (Å)	3.0-6.0	3.0-6.0
Refinement		
Initial model used (PDB code)	6ACU	6ACU
Model resolution (Å)	3.5	3.3
Model resolution range (Å)	Up to 3.5	Up to 3.3
Map sharpening B factor (Å²)	-114	-116
Model map FSC (masked)	0.85	0.86
Model composition		
Non-hydrogen atoms	4998	5000
Protein residues	639	637
Ligands	0	0
B factors (Å²)		
Protein	38	31
Ligand	-	-
R.m.s. deviations		
Bond lengths (Å)	0.003	0.003
Bond angles (°)	0.64	0.64
Validation		
MolProbity score	2.37	2.38
Clashscore	7.28	8.19
Poor rotamers (%)	5.11	5.47
Ramachandran plot		
Favored (%)	93.46	94.54
Allowed (%)	6.38	5.30
Disallowed (%)	0.16	0.16

Table S1. Cryo-EM data collection, refinement, and validation statistics (continued).

	CV-A10 bound to KRM1 (pH 7.4)	CV-A10 bound to KRM1 (pH 5.5)
Data collection and processing		
Magnification	37879	37879
Voltage (kV)	200	200
Electron exposure (e$^-$/Å^2)	40	40
Defocus range (μm)	-1.5 to -2.5	-1.5 to -2.5
Pixel size (Å)	1.32	1.32
Symmetry imposed	Icosahedral	Icosahedral
Initial particle images (no.)	46698	25058
Final particle images (no.)	28084	17659
Map resolution (Å)	3.0	3.0
FSC threshold	0.143	0.143
Map resolution range (Å)	3.0-6.0	3.0-6.0
Refinement		
Initial model used (PDB code)	6ACU, 5FWS	6ACU, 5FWS
Model resolution (Å)	3.1	3.1
Model resolution range (Å)	Up to 3.0	Up to 3.0
Map sharpening B factor (Å^2)	-107	-88
Model map FSC (masked)	0.84	0.85
Model composition		
Non-hydrogen atoms	8586	8557
Protein residues	1094	1093
Ligands	4	3
B factors (Å^2)		
Protein	33	50
Ligand	60	98
R.m.s. deviations		
Bond lengths (Å)	0.003	0.003
Bond angles (°)	0.59	0.56
Validation		
MolProbity score	2.49	2.28
Clashscore	8.69	6.33
Poor rotamers (%)	6.05	4.65
Ramachandran plot		
Favored (%)	93.36	93.54
Allowed (%)	6.55	6.37
Disallowed (%)	0.09	0.09

Table S2. Atomic contacts between KRM1 and CV-A10 VPs at pH 5.5.

KRM1	Contacts	VP1.1	Total Contacts
H126	3*	T163(1)^	
N140	1	T209	9
H194	4, 1	S217, T219	
KRM1	**Contacts**	**VP2.1**	**Total Contacts**
P65	1	N138	
Y66	5	E143	
D88	2, 5	K140(1), E143	
D90	1, 5	K140(1), N142(1)	32
Y105	4, 1	T139(1), K140	
W106	7, 1	K140, P141	
KRM1	**Contacts**	**VP3.1**	**Total Contacts**
G103	4	V238	4
KRM1	**Contacts**	**VP1.2**	**Total Contacts**
G127	1	R288	
N128	5	R288	
G134	2	D289	
T135	1	D289, R290	
S136	2	D289	22
T138	6	N297	
F150	1	S291	
Q154	4	S291(1)	
KRM1	**Contacts**	**VP3.2**	**Total Contacts**
H126	4	T234	
G127	5	T234	
N128	7	E232	40
T138	1	R90(1)	

N140	3, 4	G182(1), D185(1)	
Y165	1, 6, 7	T180, G181, G182	
F191	2	N183	

*Numbers represent the number of atom-to-atom contacts between the KRM1 residues and CV-A10 VP residues, which were analyzed by the contact program in the CCP4 suite (the distance cutoff was 4.0 Å).

^Numbers in the parentheses represent the number of potential hydrogen bonds between the nitrogen and oxygen atoms is less than 3.5 Å.